

# Quantum violation of local causality in urban network with hybrid photonic technologies

Gonzalo Carvacho,<sup>1,\*</sup> Emanuele Roccia,<sup>1,\*</sup> Mauro Valeri,<sup>1</sup> Francesco Basso Basset,<sup>1</sup> Davide Poderini,<sup>1</sup> Claudio Pardo,<sup>1</sup> Emanuele Polino,<sup>1</sup> Lorenzo Carosini,<sup>1</sup> Michele B. Rota,<sup>1</sup> Julia Neuwirth,<sup>1</sup> Saimon F. Covre da Silva,<sup>2</sup> Armando Rastelli,<sup>2</sup> Nicolò Spagnolo,<sup>1</sup> Rafael Chaves,<sup>3</sup> Rinaldo Trotta,<sup>1,†</sup> and Fabio Sciarrino<sup>1,‡</sup>

<sup>1</sup>*Dipartimento di Fisica - Sapienza Università di Roma, P.le Aldo Moro 5, I-00185 Roma, Italy*

<sup>2</sup>*Institute of Semiconductor and Solid State Physics, Johannes Kepler University, 4040 Linz, Austria*

<sup>3</sup>*International Institute of Physics and School of Science and Technology,  
Federal University of Rio Grande do Norte, 59078-970, P. O. Box 1613, Natal, Brazil*

(Dated: February 6, 2022)

Quantum networks play a crucial role for distributed quantum information processing, enabling the establishment of entanglement and quantum communication among distant nodes. Fundamentally, networks with independent sources allow for new forms of nonlocality, beyond the paradigmatic Bell's theorem. Here we implement the simplest of such networks –the bilocality scenario– in an urban network connecting different buildings with a fully scalable and hybrid approach. Two independent sources using different technologies, respectively a quantum dot and a nonlinear crystal, are used to share photonic entangled state among three nodes connected through a 270 m free-space channel and fiber links. By violating a suitable non-linear Bell inequality, we demonstrate the nonlocal behaviour of the correlations among the nodes of the network. Our results pave the way towards the realization of more complex networks and the implementation of quantum communication protocols in an urban environment, leveraging on the capabilities of hybrid photonic technologies.

*Introduction* – In the last decade, several breakthroughs on quantum communication have been reported, especially those regarding the experimental realization of quantum networks [1–4]. Quantum key distribution on fiber networks have demonstrated the possibility to securely connect distances greater than 400 km [5–7] and the successful launch of a satellite allowed the first quantum network covering record distances over 4,600 km, integrating space-to-ground and optical fibers communication [8]. At the basis of many of these quantum communication protocols is the phenomenon of Bell nonlocality [9–11], arguably the most radical departure between classical and quantum descriptions of nature. Besides its profound foundational implications, generating nonlocal correlations has become of crucial importance for a variety of quantum technologies, ranging from distributed computing [12], quantum cryptography [13–19] and quantum key distribution [20, 21] to randomness generation [22–24] and self-testing [25, 26].

Despite the apparent simplicity of Bell's theorem [9], it took over fifty years for the first loophole-free violation of a Bell inequality [27–29]. This has been achieved considering the simplest Bell scenario where a single source distributes entangled pairs among two distant nodes. Within this context, nonlocal correlations have been obtained using free-space links [30–33], fiber-based links [34–39], and satellite-based communications [40–43]. Moving beyond the paradigmatic Bell scenario, it has been realized that nonlocality can also arise in more complex networks, where the correlations between the distant nodes are mediated by a number of independent sources and in a variety of topologies. Motivated by a causality perspective [44] showing, in particular that Bell's theorem can be seen as a particular case of a causal inference problem [45, 46], quantum networks of growing size and complexity have been attracting a growing theoretical interest [47–60].

In spite of its clear foundational and technological relevance, however, the experimental investigation of these new forms of nonlocality [61–70] have been hampered by difficulties arising from quantum networks. Indeed, in order to realize large scale quantum networks and exploit them for practical tasks [4, 71], it is crucial to extend their implementation to urban scale scenarios. With that aim, two requirements have to be satisfied. First, the experimental apparatus should be scalable, such that connecting an increasing number of distant nodes is within technological reach. Second, the possibility to interface or merge different quantum technologies and types of communication links.

In this work, we take a significant step in this direction, by experimentally realizing a bilocal network [47, 48, 61, 63–65], a scenario akin to the paradigmatic entanglement swapping protocol [72, 73]. Importantly, differently from previous experiments, we generate nonlocal correlations in this network through a scalable and hybrid photonic platform composed of two photonic sources distributing photons among three nodes. In contrast with implementations that rely on entangled measurements, a demanding task in linear optics [74–76], we exploit separable measurements only, allowing the scalability of our approach to networks of increasing size. Notably, the independent sources of quantum entanglement employ two radically different technologies: Spontaneous Parametric Down Conversion (SPDC) and a quantum dot (QD). SPDC represents the most used process for the generation of polarization entangled photon pairs [77], providing high quality entangled states which can be generated in a compact and cost-effective system. In turn, QD is one of the most promising platforms for realizing deterministic photon sources [78]. Complementing the truly hybrid nature of our experiment, we simultaneously employ a fiber-based as well as free-space communication link, arguably the main kinds of communication channels to be used in future urban quantum networks. In

particular, the free-space link is a 270 m long connection between two buildings at the campus of Sapienza University of Rome. By violating a Bell inequality suited for the bilocal scenario, we demonstrate the nonlocal nature of the correlations generated among the nodes of the network. This is achieved in the so-called device independent paradigm [79–84], that is, without assuming any knowledge of the inner workings of the sources, measurement stations and other devices. In this way, we provide a reliable and versatile platform for a urban quantum network, feasible to be extended to complex scenarios with larger number of nodes, sources and covering larger distances.

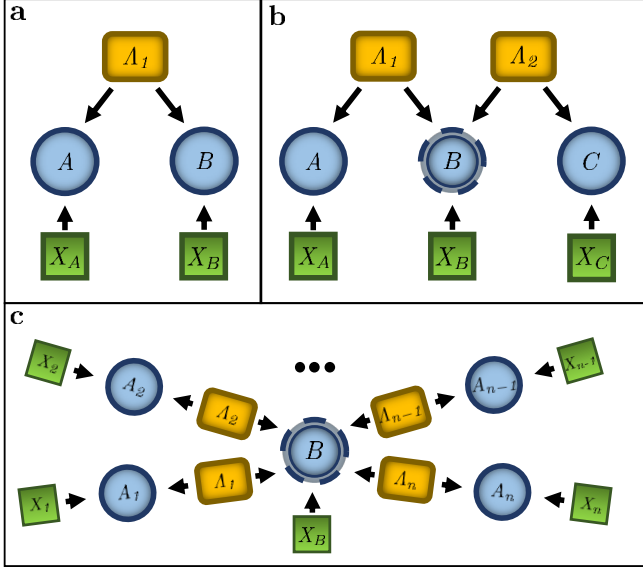


**FIG. 1. Directed acyclic graph representation of different causal structures.** Examples of network where  $n$ -nodes are connected to a central one by means of intermediate nodes, i.e., the star-shape network (SSN)[65]. **a)** Standard Bell scheme. **b)** Bilocal scenario. **c)** General SSN scheme. Independent sources of correlations ( $\Lambda_1, \dots, \Lambda_n$ ) connect peripheral nodes ( $A_1, \dots, A_n$ ) to a central one ( $B$ ). The measurement performed by the nodes are also influenced by their measurement choices ( $X_B, X_1, \dots, X_n$ ). In particular, the central node  $B$  consists of different measurement setups which are influenced by different sources,  $\Lambda_1, \dots, \Lambda_n$ , and the same measurement choice  $X_B$ . **a)** and **b)** are particular cases of SSN having  $n = 1$  and  $n = 2$ , respectively.

**Bilocal Scenario** – In its essence, Bell’s theorem shows that the correlations obtained by measurements on distant parties of an entangled system cannot be explained by classical notions of cause and effect. In practice, we impose a given causal structure to our experiment and test whether the constraints arising from a classical description of it, the so called Bell inequalities, can be violated. The paradigmatic causal structure in Bell’s theorem is shown in Fig. 1a, represented by a directed acyclic graph (DAG), where each node defines a variable of relevance for the experiment and the directed edges encode their causal relations. In Bell’s DAG, two distant parties are connected by a single source, classically described by

a hidden variable  $\Lambda$ , originating the correlations between the measurement outcomes  $A$  and  $B$  given that the parties measure observables parametrized by  $X_A$  and  $X_B$ , respectively.

Moving beyond this simple causal structure, it has been realized that networks of different topologies involving an increasing number of nodes and independent sources can lead to new forms of nonlocality [48, 50–60], motivating a number of novel experimental implementations [61–70]. Of particular, relevance is the bilocal scenario, providing the simplest network beyond the bipartite case and that for this reason has attract significant interest [47–50, 61–65]. Its causal structure is represented by the DAG in Fig. 1b, where two nodes ( $A, C$ ) are connected with a central one ( $B$ ), by means of two independent sources of correlations ( $\Lambda_1, \Lambda_2$ ) [85].

The classical description of the bilocal scenario is uniquely defined by the Markov condition [44], which constrains the conditional probabilities of the measurement outcomes as

$$p(a, b, c | x_A, x_B, x_C) = \sum_{\lambda_1, \lambda_2} p(\lambda_1) p(\lambda_2) \times \times p(x_1 | x_A, \lambda_A) p(x_B | x_B, \lambda_2) p(x_C | x_C, \lambda_1, \lambda_2), \quad (1)$$

in which the independence of the sources of shared randomness implies the non-linear condition  $p(\lambda_1, \lambda_2) = p(\lambda_1) p(\lambda_2)$ . If one out of two possible dichotomic measurements is performed, that is,  $a, b, c \in \{0, 1\}$  and  $x_A, x_B, x_C \in \{0, 1\}$ , the classical description (1) implies that the observed correlations should respect a non-linear Bell inequality given by [47, 48, 53, 86, 87]

$$B = \sqrt{|I_1|} + \sqrt{|I_2|} \leq 1. \quad (2)$$

where

$$I_1 = \frac{1}{4} \sum_{x_A, x_B} \langle A^{x_A} B^{x_B} C^0 \rangle, \\ I_2 = \frac{1}{4} \sum_{x_A, x_B} (-1)^{x_A + x_B} \langle A^{x_A} B^{x_B} C^1 \rangle, \\ \langle A^{x_A} B^{x_B} C^{x_C} \rangle = \sum_{a, b, c} (-1)^{a+b+c} p(a, b, c | x_A, x_B, x_C). \quad (3)$$

In a quantum description of the bilocal experiment, the two sources are represented by bipartite quantum states  $\rho_1$  and  $\rho_2$  and the measurements are given by observables defined by operators  $\hat{A}^{x_A}, \hat{B}^{x_B}, \hat{C}^{x_C}$  acting on their respective subsystem. The corresponding probability distribution of measurement outcomes are given, according to the Born’s rule, by  $p(a, b, c | x_A, x_B, x_C) = \text{Tr} \left[ \left( \hat{A}^{x_A} \otimes \hat{B}^{x_B} \otimes \hat{C}^{x_C} \right) (\rho_1 \otimes \rho_2) \right]$ . As demonstrated by several works using photonic platforms [61–64], by properly choosing the quantum states and measurements, the bilocal inequality (2) can be violated, showing the incompatibility between classical causality and quantum predictions also in this new kind of causal network. Remarkably, adopting separable measurements in the central node  $B$  it is also possible

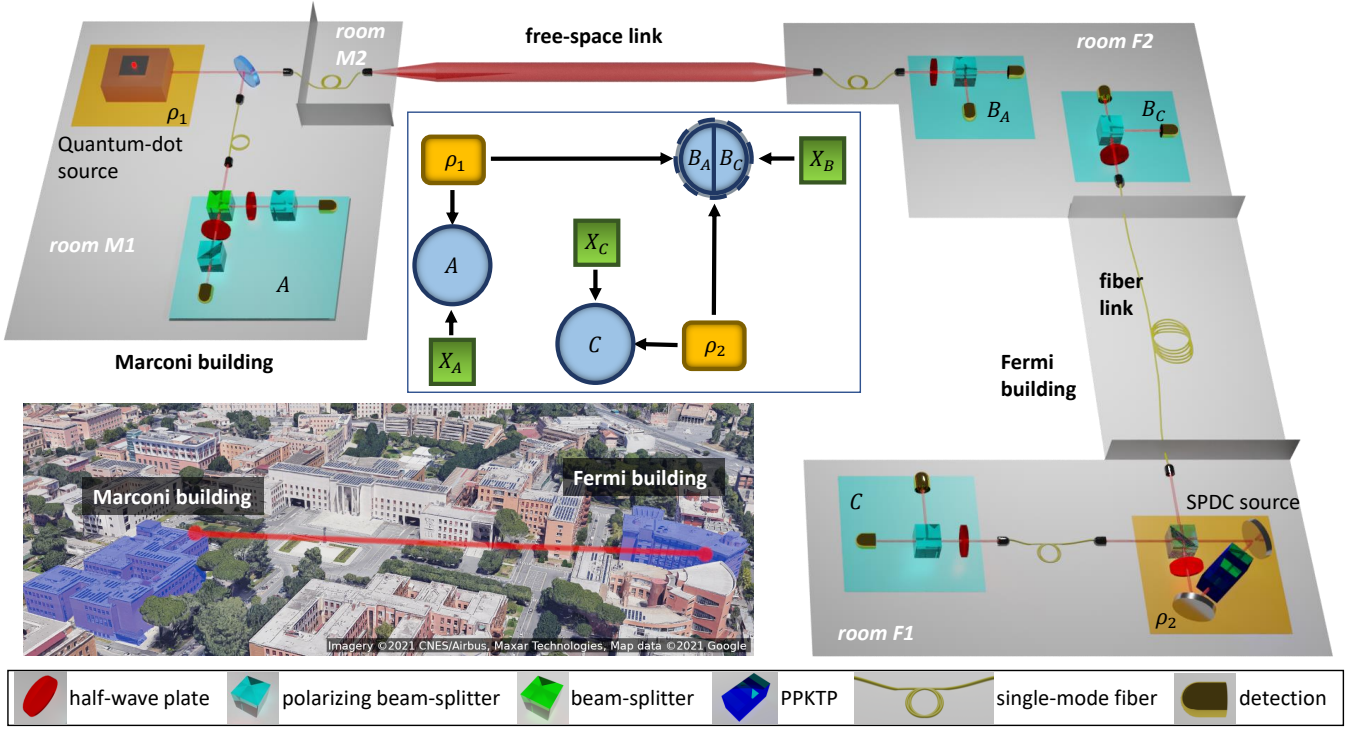


FIG. 2. **Experimental implementation of the quantum network.** To realize the bilocal scenario, multiple laboratories located in different rooms and buildings were used. In particular, two sources of polarization-entangled photon pairs are realized via quantum dot device and SPDC in a Sagnac interferometer. They are placed inside the laboratories of two different buildings, respectively, the Marconi and the Fermi buildings. The entanglement is distributed from such laboratories to a central one — place in the Fermi building — by using a free space channel and a fiber link. A dedicated stabilization system was employed to use the free-space link (not shown in the figure). The corresponding bilocal scheme in DAG representation is reported in the middle: according to Fig.1b, two independent sources of correlations ( $\rho_1, \rho_2$ ) connect two external nodes (A,C) to a central one (B). The two measurement setups influenced by the different sources are indicated as  $B_A$  and  $B_C$ .

to violate such inequalities [48, 63, 65, 88, 89]. In particular, when singlet quantum states,  $|\Psi_1^-\rangle$  and  $|\Psi_2^-\rangle$ , are prepared by the two sources and distributed between the parties, a maximum violation of the bilocal Bell-like inequality can be obtained  $\mathcal{B}_Q^{\max} = \sqrt{2} \approx 1.414$ . This value is achieved by considering two separable observables in the central node B, which measure the subsystems of the singlet state shared with A and C:  $\hat{B}^{x_B} = \hat{B}_A^{x_B} \otimes \hat{B}_C^{x_B}$ . Both observables can be taken as Pauli matrices  $\sigma_z$  and  $\sigma_x$ . While each of the external nodes measures  $(\sigma_x + \sigma_z)/\sqrt{2}$  and  $(\sigma_x - \sigma_z)/\sqrt{2}$ . This condition of separable measurements is particularly suitable to guarantee the scalability of the network, since it can be implemented using independent photonic platforms without the stringent requirements needed to perform entangled measurements. This is precisely our case, where we even adopt different quantum emitters of single photons, a SPDC source and a QD pumped by independent lasers working in continuous and pulsed mode, respectively. Importantly, the violation of the bilocality inequality (2) is possible even if the distribution  $p(a, b, c | x_A, x_B, x_C)$  does not violate any standard Bell inequality. For instance, the choices of states and measurements described above and that will be used in our experimental implementation, cannot violate the Clauser-Horne-Shimony-

Holt (CHSH) inequality [90] between stations A and B, given by

$$S_{AB} = \sum_{x_A, x_B} (-1)^{x_A x_B} \langle A^{x_A} B^{x_B} \rangle \leq 2, \quad (4)$$

and similarly cannot violate the corresponding CHSH inequality between stations B and C. That is, the non-classicality of the considered statistics truly requires the test of the underlying bilocality network to be detected.

*Experimental apparatus* – In the following we discuss the photonic platform implementing bilocality network and achieving the violation of the inequality (2). See Fig. 2 for details.

One of the sources ( $\rho_1$ ) of polarization-entangled photons is composed by a single GaAs QD in a matrix of  $\text{Al}_{0.4}\text{Ga}_{0.6}\text{As}$ . The quantum dots are fabricated with the Al droplet etching method and are placed between two asymmetric distributed Bragg reflectors, as detailed in [91]. Using a Weierstrass solid immersion lens and an aspheric lens for collection, the extraction efficiency is approximately 10%. The QD is optically pumped under resonant two-photon excitation [92] at 782.2 nm with a laser repetition rate of 320 MHz. The rate of measured coincidence events at the output of the source is 13.7 kHz. The QD is selected with a low fine-structure splitting

(FSS) of  $0.8 \pm 0.5 \mu\text{eV}$  to achieve a measured fidelity to a maximally entangled state of  $0.929 \pm 0.004$ , without the need for temporal or spectral filtering. The CHSH parameter (4) measured is  $S_{\text{QD}} = 2.66 \pm 0.02$ . Using a set of wave plates we maximize the fidelity of the photon pairs to the singlet state in polarization.

Regarding the SPDC source ( $\rho_2$ ), entangled photon pairs in polarization are generated pumping a nonlinear ppKTP crystal placed into a Sagnac interferometer. The continuous-wave pump has a frequency of 405 nm, while the signal-idler generation is degenerate at 810 nm. The rate of measured coincidence events between the two output modes is 3 kHz. The final state is properly tuned by a polarization controller in order to obtain singlet states in polarization,  $|\Psi^-\rangle$ , along the two output modes (1,2). The CHSH parameter (4) measured at the output of the source, i.e. before distributing the photons, is  $S_{\text{SPDC}} = 2.727 \pm 0.007$  without accidental correction of the data. The estimated state fidelity with respect to the singlet state is  $0.955 \pm 0.001$ . In addition, the source is mounted in a compact and monolithic architecture (see Supplemental Material) providing high stability of the generated signal, as well as enabling the possibility to transfer and operate the source in different locations.

Using these sources of photonic entanglement, the implemented quantum bilocal network is reported in Fig. 2. The source  $\rho_1(\rho_2)$  is shared between external A(C) and the central node B. The two sources are located near the corresponding peripheral nodes, i.e. source  $\rho_1(\rho_2)$  is in the same laboratory as the measurement station A(C). Two stations, B and C, are placed in two distinct laboratories inside the same building, and are connected through a 25 m long single mode fiber. The other station A is placed in a different building 270 m apart from the one of B and C. This node is connected to the central one (B) through a free-space channel stabilized by means of dedicated system using the feedback from an additional reference laser at 850 nm and a couple of piezoelectric mirrors at the receiver to counter the effects of atmospheric turbulence and beam wander [33], plus a piezoelectric mirror at the sender to remove thermal drifts in the pointing direction (see Supplemental Material). Stations C and B are also equipped with a GPS-locked oscillator, used to generate the common clock signal necessary for the synchronization of the detection events between the two buildings. The system also exploits the two-fold coincidences events between C and B to obtain the required accuracy. In order to realize the optimal measurements, each station is equipped with standard setups for linear polarization measurement, consisting of a half wave plate (HWP) and polarizing beam splitter (PBS). Specifically, in the external nodes, A and C, the two basis required are realized by setting the HWP at  $11.25^\circ (= \pi/16)$  and  $33.75^\circ (= 3\pi/16)$ . Conversely, in the central node B, the measurements performed on the photons coming from the two quantum channels are realized using two independent measurement setups. In both these setups, it is sufficient to set the HWP at angles  $0^\circ$  and  $22.5^\circ (= \pi/8)$ .

**Results** – Each observable of the tripartite system ABC

requires the simultaneous detection of four-fold coincidence events. In order to achieve this, we first record two-fold events of subsystems AB and BC, independently. Then, four-fold events are recovered by filtering all the two-fold data inside a given time window. This procedure allows us to considerably reduce background noise while retaining an optimal rate for the four-fold events. The size of the window can be tuned, thus varying the statistics and the considered simultaneity of the events, similarly to [65]. The analysis of the violation of Eq.(2) is reported in Fig. 3, where optimal performances are reached for the window  $51.435 \mu\text{s}$ . Using this window, we obtain a mean value of  $\mathcal{B}_{\text{exp}} = 1.312 \pm 0.0052$  averaged over  $\sim 25$  minutes. Further, two-fold events can be processed to extract the values of Bell parameters distributed along the quantum channels during the bilocality experiment. The analysis provides CHSH violations of  $S_{\text{AB}} = 2.484 \pm 0.018$  and  $S_{\text{BC}} = 2.699 \pm 0.006$  for the QD and the SPDC source, respectively. The time trend of CHSH and bilocality violation of our network can be found in Supplemental Material. Notably, we obtain a violation of the classical limit also with windows in the range 300–800 ns which, in principle, allows the events in nodes A and B to be recorded with space-like separations with respect to C, partially addressing the locality loophole of our implementation.

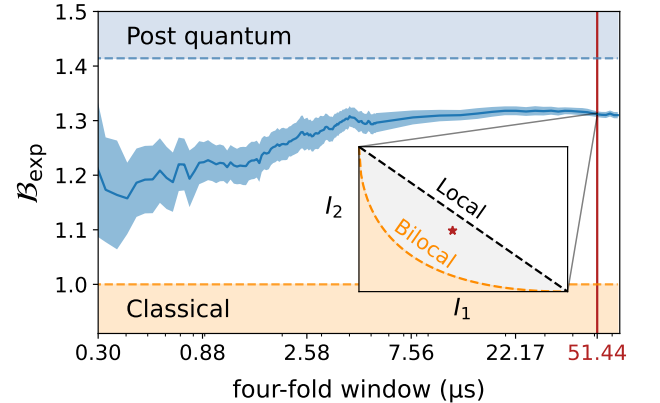


**FIG. 3. Experimental results.** Quantum violation  $\mathcal{B}_{\text{exp}}$  of the Bell-like inequality for the bilocal scenario is shown as a function of the time window in which four-fold coincidence events are considered simultaneous. The dashed orange and blue lines represent the classical and the quantum bounds,  $\mathcal{B}_{\text{cl}} = 1$  and  $\mathcal{B}_{\text{Q}} = \sqrt{2}$  respectively, while the solid blue line indicates the measured value of  $\mathcal{B}_{\text{exp}}$  with the corresponding error represented by the light blue area. The error is computed through repeated measurements over  $\sim 25$  minutes. While the optimal value, in terms of  $\sigma$ -distance from the bound, is reached using a window of  $51.4350 \mu\text{s}$ , a significant violation can be obtained also considering much smaller windows, up to 283.5 ns. In the inset, the point corresponding to the optimal window of  $51.4350 \mu\text{s}$  is shown in the space of correlations  $I_1, I_2$ , as defined in Eq. (3), where the classical bound corresponding to the bilocal scenario is represented by the green area, while the gray area represents the classical correlations allowed by the relaxed scenario in which the assumption of independence of the source is lifted, corresponding to a tripartite Bell scenario.

**Conclusions** – A crucial requirement for the development of quantum communication networks is the ability to exploit and combine widely different technologies that are currently available, in a modular and reliable way. In this direction, we experimentally demonstrated the quantum violation of local causality in a hybrid tripartite quantum network. We violate a bilocality inequality, surpassing the classical bound by more than 60 standard deviations and thus prove the emergence of nonclassical correlations that could not be detected by standard Bell inequalities. Our network is composed of three nodes interconnected by fiber and free-space photonic links and two distinct sources of entangled photons. The two sources are based on significantly different technologies: a SPDC-based generation at 810 nm pumped by 405 nm cw-laser and a quantum dot emission at 781.2–783.2 nm pumped in pulsed regime. Thus, our platform employs two intrinsically independent sources, a fundamental requirement for testing classical bounds in networks such as the bilocality scenario and others of increasing size and number of sources. Furthermore, we studied the violation of the Bell-like inequality for such scenario, tuning the time window in which four-fold coincidence events are considered simultaneous, including time windows in which the events in the distant stations can be considered space-like separated, an important ingredient for a fully loophole free demonstration. This work shows the reliability and versatility of the implemented platform, merging and interfacing technologically different solutions in the same network. The use of separable measurements allows interfacing sources of different natures, avoiding the drawbacks of optical Bell-state measurements requiring also the synchronization of the single-photon emission [93]. Furthermore, our experiment has employed both free-space and fiber links in an urban environment, whose combined adoption represent a crucial requirement towards large scale networks. All these features demonstrate that our approach can be easily applied and scaled to any complex causal network, and can be used as a building block for future real-life quantum secure communication networks based on quantum nonlocality.

**Acknowledgements** – This work was financially supported by the European Research Council (ERC) under the European Union’s Horizon 2020 Research and Innovation Programme (SPQRel, grant agreement no. 679183), and by MIUR (Ministero dell’Istruzione, dell’Università e della Ricerca) via project PRIN 2017 “Taming complexity via Quantum Strategies a Hybrid Integrated Photonic approach” (QUSHIP) Id. 2017SRNBRK. We acknowledge support from The John Templeton Foundation via the grant Q-CAUSAL No. 61084 and via The Quantum Information Structure of Spacetime (QISS) Project (qiss.fr) Grant Agreement No. 61466 (the opinions expressed in this publication are those of the authors and do not necessarily reflect the views of The John Templeton Foundation). This project has received funding from the European Union’s Horizon 2020 Research and Innovation Program under Grant Agreement no. 899814 (Quore). RC also acknowledges the Serrapilheira Institute (Grant No. Serra-1708-15763), the Brazilian National Council for Scien-

tific and Technological Development (CNPq) via the INCT-IQ and Grants No. 307172/2017-1 and No. 311375/2020-0.

---

\* These two authors contributed equally

† rinaldo.trotta@uniroma1.it

‡ fabio.sciarrino@uniroma1.it

- [1] Nicolas Gisin and Rob Thew, “Quantum communication,” *Nature photonics* **1**, 165–171 (2007).
- [2] Hoi-Kwong Lo, Marcos Curty, and Kiyoshi Tamaki, “Secure quantum key distribution,” *Nature Photonics* **8**, 595–604 (2014).
- [3] Eleni Diamanti, Hoi-Kwong Lo, Bing Qi, and Zhiliang Yuan, “Practical challenges in quantum key distribution,” *npj Quantum Information* **2**, 1–12 (2016).
- [4] Stephanie Wehner, David Elkouss, and Ronald Hanson, “Quantum internet: A vision for the road ahead,” *Science* **362** (2018).
- [5] Jiu-Peng Chen, Chi Zhang, Yang Liu, Cong Jiang, Weijun Zhang, Xiao-Long Hu, Jian-Yu Guan, Zong-Wen Yu, Hai Xu, Jin Lin, *et al.*, “Sending-or-not-sending with independent lasers: Secure twin-field quantum key distribution over 509 km,” *Physical review letters* **124**, 070501 (2020).
- [6] Alberto Boaron, Gianluca Boso, Davide Rusca, Cédric Vulliez, Claire Autebert, Misael Caloz, Matthieu Perrenoud, Gaëtan Gras, Félix Bussi eres, Ming-Jun Li, *et al.*, “Secure quantum key distribution over 421 km of optical fiber,” *Physical review letters* **121**, 190502 (2018).
- [7] Hua-Lei Yin, Teng-Yun Chen, Zong-Wen Yu, Hui Liu, Li-Xing You, Yi-Heng Zhou, Si-Jing Chen, Yingqiu Mao, Ming-Qi Huang, Wei-Jun Zhang, *et al.*, “Measurement-device-independent quantum key distribution over a 404 km optical fiber,” *Physical review letters* **117**, 190501 (2016).
- [8] Yu-Ao Chen, Qiang Zhang, Teng-Yun Chen, Wen-Qi Cai, Sheng-Kai Liao, Jun Zhang, Kai Chen, Juan Yin, Ji-Gang Ren, Zhu Chen, *et al.*, “An integrated space-to-ground quantum communication network over 4,600 kilometres,” *Nature* **589**, 214–219 (2021).
- [9] John S Bell, “On the einstein podolsky rosen paradox,” *Physics Physique Fizika* **1**, 195 (1964).
- [10] Nicolas Brunner, Daniel Cavalcanti, Stefano Pironio, Valerio Scarani, and Stephanie Wehner, “Bell nonlocality,” *Reviews of Modern Physics* **86**, 419 (2014).
- [11] Valerio Scarani, *Bell nonlocality* (Oxford University Press, 2019).
- [12] Harry Buhrman, Richard Cleve, Serge Massar, and Ronald de Wolf, “Nonlocality and communication complexity,” *Rev. Mod. Phys.* **82**, 665–698 (2010).
- [13] Nicolas Gisin, Gr egoire Ribordy, Wolfgang Tittel, and Hugo Zbinden, “Quantum cryptography,” *Rev. Mod. Phys.* **74**, 145–195 (2002).
- [14] Artur K. Ekert, “Quantum cryptography based on bell’s theorem,” *Phys. Rev. Lett.* **67**, 661–663 (1991).
- [15] Thomas Jennewein, Christoph Simon, Gregor Weihs, Harald Weinfurter, and Anton Zeilinger, “Quantum cryptography with entangled photons,” *Phys. Rev. Lett.* **84**, 4729–4732 (2000).
- [16] Christian Schimpf, Marcus Reindl, Daniel Huber, Barbara Lehner, Simon F. Cove da Silva, Michal Vyb lecka, Philip Walther, and Armando Rastelli, “Quantum cryptography with highly entangled photons from semiconductor quantum dots,” *Science Advances* **7**, 10.1126/sciadv.abe8905.
- [17] Artur K Ekert, “Quantum cryptography based on bell’s theo-



- rem,” *Physical review letters* **67**, 661 (1991).
- [18] Valerio Scarani, Helle Bechmann-Pasquinucci, Nicolas J Cerf, Miloslav Dušek, Norbert Lütkenhaus, and Momtchil Peev, “The security of practical quantum key distribution,” *Reviews of modern physics* **81**, 1301 (2009).
  - [19] Feihu Xu, Xiongfeng Ma, Qiang Zhang, Hoi-Kwong Lo, and Jian-Wei Pan, “Secure quantum key distribution with realistic devices,” *Reviews of Modern Physics* **92**, 025002 (2020).
  - [20] Jonathan Barrett, Lucien Hardy, and Adrian Kent, “No signaling and quantum key distribution,” *Phys. Rev. Lett.* **95**, 010503 (2005).
  - [21] Antonio Acín, Nicolas Gisin, and Lluís Masanes, “From bell’s theorem to secure quantum key distribution,” *Phys. Rev. Lett.* **97**, 120405 (2006).
  - [22] S. Pironio, A. Acín, S. Massar, A. Boyer de la Giroday, D. N. Matsukevich, P. Maunz, S. Olmschenk, D. Hayes, L. Luo, T. A. Manning, and C. Monroe, “Random numbers certified by bell’s theorem,” *Nature* **464**, 1021–1024 (2010).
  - [23] Yang Liu, Qi Zhao, Ming-Han Li, Jian-Yu Guan, Yanbao Zhang, Bing Bai, Weijun Zhang, Wen-Zhao Liu, Cheng Wu, Xiao Yuan, Hao Li, W. J. Munro, Zhen Wang, Lixing You, Jun Zhang, Xiongfeng Ma, Jingyun Fan, Qiang Zhang, and Jian-Wei Pan, “Device-independent quantum random-number generation,” *Nature* **562**, 548–551 (2018).
  - [24] Iris Agresti, Davide Poderini, Leonardo Guerini, Michele Mancusi, Gonzalo Carvacho, Leandro Aolita, Daniel Cavalcanti, Rafael Chaves, and Fabio Sciarrino, “Experimental device-independent certified randomness generation with an instrumental causal structure,” *Communications Physics* **3**, 110 (2020).
  - [25] Ivan Šupić and Joseph Bowles, “Self-testing of quantum systems: a review,” *Quantum* **4**, 337 (2020).
  - [26] Iris Agresti, Beatrice Polacchi, Davide Poderini, Emanuele Polino, Alessia Suprano, Ivan Šupić, Joseph Bowles, Gonzalo Carvacho, Daniel Cavalcanti, and Fabio Sciarrino, “Experimental robust self-testing of the state generated by a quantum network,” *PRX Quantum* **2**, 020346 (2021).
  - [27] Marissa Giustina, Marijn AM Versteegh, Soren Wengerowsky, Johannes Handsteiner, Armin Hochrainer, Kevin Phelan, Fabian Steinlechner, Johannes Kofler, Jan-AAke Larsson, Carlos Abell’an, *et al.*, “Significant-loophole-free test of Bell’s theorem with entangled photons,” *Phys. Rev. Lett.* **115**, 250401 (2015).
  - [28] Lynden K Shalm, Evan Meyer-Scott, Bradley G Christensen, Peter Bierhorst, Michael A Wayne, Martin J Stevens, Thomas Gerrits, Scott Glancy, Deny R Hamel, Michael S Allman, *et al.*, “Strong loophole-free test of local realism,” *Phys. Rev. Lett.* **115**, 250402 (2015).
  - [29] Bas Hensen, Hannes Bernien, Anais E Dr’eau, Andreas Reiserer, Norbert Kalb, Machiel S Blok, Just Ruitenberg, Raymond FL Vermeulen, Raymond N Schouten, Carlos Abell’an, W. Amaya, V. Pruneri, M. W. Mitchell, M. Markham, D. J. Twitchen, D. Elkouss, S. Wehner, T. H. Taminiau, and R. Hanson, “Loophole-free Bell inequality violation using electron spins separated by 1.3 kilometres,” *Nature* **526**, 682 (2015).
  - [30] Cheng-Zhi Peng, Tao Yang, Xiao-Hui Bao, Jun Zhang, Xian-Min Jin, Fa-Yong Feng, Bin Yang, Jian Yang, Juan Yin, Qiang Zhang, *et al.*, “Experimental free-space distribution of entangled photon pairs over 13 km: towards satellite-based global quantum communication,” *Physical review letters* **94**, 150501 (2005).
  - [31] Xiao-Song Ma, Thomas Herbst, Thomas Scheidl, Daqing Wang, Sebastian Kropatschek, William Naylor, Bernhard Wittmann, Alexandra Mech, Johannes Kofler, Elena Anisimova, *et al.*, “Quantum teleportation over 143 kilometres using active feed-forward,” *Nature* **489**, 269–273 (2012).
  - [32] Juan Yin, Ji-Gang Ren, He Lu, Yuan Cao, Hai-Lin Yong, Yu-Ping Wu, Chang Liu, Sheng-Kai Liao, Fei Zhou, Yan Jiang, *et al.*, “Quantum teleportation and entanglement distribution over 100-kilometre free-space channels,” *Nature* **488**, 185–188 (2012).
  - [33] Francesco Basso Basset, Mauro Valeri, Emanuele Roccia, Valerio Muredda, Davide Poderini, Julia Neuwirth, Nicolò Spagnolo, Michele B Rota, Gonzalo Carvacho, Fabio Sciarrino, *et al.*, “Quantum key distribution with entangled photons generated on demand by a quantum dot,” *Science Advances* **7**, eabe6379 (2021).
  - [34] Sören Wengerowsky, Siddarth Koduru Joshi, Fabian Steinlechner, Julien R Zichi, Sergiy M Dobrovolskiy, René van der Molen, Johannes WN Los, Val Zwiller, Marijn AM Versteegh, Alberto Mura, *et al.*, “Entanglement distribution over a 96-km-long submarine optical fiber,” *Proceedings of the National Academy of Sciences* **116**, 6684–6688 (2019).
  - [35] Takuya Ikuta and Hiroki Takesue, “Four-dimensional entanglement distribution over 100 km,” *Scientific reports* **8**, 1–7 (2018).
  - [36] James F Dynes, Hiroki Takesue, Zhiliang L Yuan, Andrew W Sharpe, K Harada, Toshimori Honjo, Hidehiko Kamada, Osamu Tadanaga, Yoshiki Nishida, Masaki Asobe, *et al.*, “Efficient entanglement distribution over 200 kilometers,” *Optics express* **17**, 11440–11449 (2009).
  - [37] Takahiro Inagaki, Nobuyuki Matsuda, Osamu Tadanaga, Masaki Asobe, and Hiroki Takesue, “Entanglement distribution over 300 km of fiber,” *Optics express* **21**, 23241–23249 (2013).
  - [38] Daniele Cozzolino, Emanuele Polino, Mauro Valeri, Gonzalo Carvacho, Davide Bacco, Nicolò Spagnolo, Leif KK Oxenløwe, and Fabio Sciarrino, “Air-core fiber distribution of hybrid vector vortex-polarization entangled states,” *Advanced Photonics* **1**, 046005 (2019).
  - [39] Christian Schimpf, Marcus Reindl, Daniel Huber, Barbara Lehner, Saimon F. Covre Da Silva, Santanu Manna, Michal Vybílecka, Philip Walther, and Armando Rastelli, “Quantum cryptography with highly entangled photons from semiconductor quantum dots,” *Science Advances* **7**, eabe8905 (2021).
  - [40] Juan Yin, Yuan Cao, Yu-Huai Li, Sheng-Kai Liao, Liang Zhang, Ji-Gang Ren, Wen-Qi Cai, Wei-Yue Liu, Bo Li, Hui Dai, *et al.*, “Satellite-based entanglement distribution over 1200 kilometers,” *Science* **356**, 1140–1144 (2017).
  - [41] Robert Bedington, Juan Miguel Arrazola, and Alexander Ling, “Progress in satellite quantum key distribution,” *npj Quantum Information* **3**, 1–13 (2017).
  - [42] Ji-Gang Ren, Ping Xu, Hai-Lin Yong, Liang Zhang, Sheng-Kai Liao, Juan Yin, Wei-Yue Liu, Wen-Qi Cai, Meng Yang, Li Li, *et al.*, “Ground-to-satellite quantum teleportation,” *Nature* **549**, 70–73 (2017).
  - [43] Juan Yin, Yu-Huai Li, Sheng-Kai Liao, Meng Yang, Yuan Cao, Liang Zhang, Ji-Gang Ren, Wen-Qi Cai, Wei-Yue Liu, Shuang-Lin Li, *et al.*, “Entanglement-based secure quantum cryptography over 1,120 kilometres,” *Nature* **582**, 501–505 (2020).
  - [44] Judea Pearl, *Causality* (Cambridge university press, 2009).
  - [45] Christopher J Wood and Robert W Spekkens, “The lesson of causal discovery algorithms for quantum correlations: Causal explanations of bell-inequality violations require fine-tuning,” *New Journal of Physics* **17**, 033002 (2015).
  - [46] Rafael Chaves, Richard Kueng, Jonatan Bohr Brask, and David Gross, “Unifying framework for relaxations of the causal assumptions in bell’s theorem,” *Physical review letters* **114**, 140403 (2015).

- [47] Cyril Branciard, Nicolas Gisin, and Stefano Pironio, “Characterizing the nonlocal correlations created via entanglement swapping,” *Phys. Rev. Lett.* **104**, 170401 (2010).
- [48] Cyril Branciard, Denis Rosset, Nicolas Gisin, and Stefano Pironio, “Bilocal versus nonbilocal correlations in entanglement-swapping experiments,” *Phys. Rev. A* **85**, 032119 (2012).
- [49] Armin Tavakoli, Nicolas Gisin, and Cyril Branciard, “Bilocal bell inequalities violated by the quantum elegant joint measurement,” *Physical Review Letters* **126**, 220401 (2021).
- [50] Marc-Olivier Renou, David Trillo, Mirjam Weilenmann, Le Phuc Thinh, Armin Tavakoli, Nicolas Gisin, Antonio Acín, and Miguel Navascués, “Quantum physics needs complex numbers,” arXiv preprint arXiv:2101.10873 (2021).
- [51] Rafael Chaves, Christian Majenz, and David Gross, “Information-theoretic implications of quantum causal structures,” *Nature communications* **6**, 1–8 (2015).
- [52] Armin Tavakoli, Paul Skrzypczyk, Daniel Cavalcanti, and Antonio Acín, “Nonlocal correlations in the star-network configuration,” *Phys. Rev. A* **90**, 062109 (2014).
- [53] Rafael Chaves, “Polynomial bell inequalities,” *Physical review letters* **116**, 010402 (2016).
- [54] Marc-Olivier Renou, Elisa Bäumer, Sadra Boreiri, Nicolas Brunner, Nicolas Gisin, and Salman Beigi, “Genuine quantum nonlocality in the triangle network,” *Phys. Rev. Lett.* **123**, 140401 (2019).
- [55] Tobias Fritz, “Beyond Bell’s theorem II: Scenarios with arbitrary causal structure,” *Communications in Mathematical Physics* **341**, 391–434 (2016).
- [56] Joe Henson, Raymond Lal, and Matthew F Pusey, “Theory-independent limits on correlations from generalized bayesian networks,” *New J. Phys.* **16**, 113043 (2014).
- [57] Elie Wolfe, Robert W Spekkens, and Tobias Fritz, “The Inflation Technique for Causal Inference with Latent Variables,” *J. Causal Inference* **7** (2019).
- [58] Nicolas Gisin, “Entanglement 25 years after quantum teleportation: testing joint measurements in quantum networks,” *Entropy* **21**, 325 (2019).
- [59] Marc-Olivier Renou, Elisa Baumer, Sadra Boreiri, Nicolas Brunner, Nicolas Gisin, and Salman Beigi, “Genuine quantum nonlocality in the triangle network,” *Phys. Rev. Lett.* **123**, 140401 (2019).
- [60] Armin Tavakoli, Alejandro Pozas-Kerstjens, Ming-Xing Luo, and Marc-Olivier Renou, “Bell nonlocality in networks,” (2021), arXiv:2104.10700 [quant-ph].
- [61] Gonzalo Carvacho, Francesco Andreoli, Luca Santodonato, Marco Bentivegna, Rafael Chaves, and Fabio Sciarrino, “Experimental violation of local causality in a quantum network,” *Nature communications* **8**, 1–6 (2017).
- [62] Dylan J Saunders, Adam J Bennet, Cyril Branciard, and Geoff J Pryde, “Experimental demonstration of nonbilocal quantum correlations,” *Science advances* **3**, e1602743 (2017).
- [63] Francesco Andreoli, Gonzalo Carvacho, Luca Santodonato, Marco Bentivegna, Rafael Chaves, and Fabio Sciarrino, “Experimental bilocality violation without shared reference frames,” *Physical Review A* **95**, 062315 (2017).
- [64] Qi-Chao Sun, Yang-Fan Jiang, Bing Bai, Weijun Zhang, Hao Li, Xiao Jiang, Jun Zhang, Lixing You, Xianfeng Chen, Zhen Wang, *et al.*, “Experimental demonstration of non-bilocality with truly independent sources and strict locality constraints,” *Nature Photonics* **13**, 687–691 (2019).
- [65] Davide Poderini, Iris Agresti, Guglielmo Marchese, Emanuele Polino, Taira Giordani, Alessia Suprano, Mauro Valeri, Giorgio Milani, Nicolò Spagnolo, Gonzalo Carvacho, *et al.*, “Experimental violation of n-locality in a star quantum network,” *Nature communications* **11**, 1–8 (2020).
- [66] Rafael Chaves, Gonzalo Carvacho, Iris Agresti, Valerio Di Giulio, Leandro Aolita, Sandro Giacomini, and Fabio Sciarrino, “Quantum violation of an instrumental test,” *Nature Physics* **14**, 291 (2018).
- [67] Emanuele Polino, Iris Agresti, Davide Poderini, Gonzalo Carvacho, Giorgio Milani, Gabriela Barreto Lemos, Rafael Chaves, and Fabio Sciarrino, “Device-independent test of a delayed choice experiment,” *Physical Review A* **100**, 022111 (2019).
- [68] G Carvacho, R Chaves, and F Sciarrino, “Perspective on experimental quantum causality,” *EPL (Europhysics Letters)* **125**, 30001 (2019).
- [69] Martin Ringbauer, Christina Giarmatzi, Rafael Chaves, Fabio Costa, Andrew G White, and Alessandro Fedrizzi, “Experimental test of nonlocal causality,” *Science advances* **2**, e1600162 (2016).
- [70] Iris Agresti, Davide Poderini, Beatrice Polacchi, Nikolai Miklin, Mariami Gachechiladze, Alessia Suprano, Emanuele Polino, Giorgio Milani, Gonzalo Carvacho, Rafael Chaves, *et al.*, “Experimental test of quantum causal influences,” arXiv preprint arXiv:2108.08926 (2021).
- [71] H Jeff Kimble, “The quantum internet,” *Nature* **453**, 1023–1030 (2008).
- [72] Marek Zukowski, Anton Zeilinger, Michael A Horne, and Arthur K Ekert, “‘‘event-ready-detectors’’ bell experiment via entanglement swapping,” *Physical Review Letters* **71** (1993).
- [73] Marek Zukowski, Anton Zeilinger, and Harald Weinfurter, “Entangling photons radiated by independent pulsed sources a,” *Annals of the New York academy of Sciences* **755**, 91–102 (1995).
- [74] N Lütkenhaus, J Calsamiglia, and K-A Suominen, “Bell measurements for teleportation,” *Physical Review A* **59**, 3295 (1999).
- [75] Lev Vaidman and Nadav Yoran, “Methods for reliable teleportation,” *Physical Review A* **59**, 116 (1999).
- [76] F. Basso Basset, F. Salusti, L. Schweickert, M. B. Rota, D. Tedeschi, S. F. Covre da Silva, E. Roccia, V. Zwiller, K. D. Jöns, A. Rastelli, and R. Trotta, “Quantum teleportation with imperfect quantum dots,” *npj Quantum Information* **7** (2021), 10.1038/s41534-020-00356-0.
- [77] Matthew D Eisaman, Jingyun Fan, Alan Migdall, and Sergey V Polyakov, “Invited review article: Single-photon sources and detectors,” *Review of scientific instruments* **82**, 071101 (2011).
- [78] Daniel Huber, Marcus Reindl, Saimon Filipe Covre Da Silva, Christian Schimpf, Javier Martín-Sánchez, Huiying Huang, Giovanni Piredda, Johannes Edlinger, Armando Rastelli, and Rinaldo Trotta, “Strain-tunable gaas quantum dot: A nearly dephasing-free source of entangled photon pairs on demand,” *Physical review letters* **121**, 033902 (2018).
- [79] Stefano Pironio, Valerio Scarani, and Thomas Vidick, “Focus on device independent quantum information,” *New Journal of Physics* **18**, 100202 (2016).
- [80] Umesh Vazirani and Thomas Vidick, “Fully device independent quantum key distribution,” *Communications of the ACM* **62**, 133–133 (2019).
- [81] Valerio Scarani, “The device-independent outlook on quantum physics,” *Acta Physica Slovaca* **62**, 347–409 (2012).
- [82] Davide Poderini, Emanuele Polino, Giovanni Rodari, Alessia Suprano, Rafael Chaves, and Fabio Sciarrino, “Ab-initio experimental violation of bell inequalities,” arXiv preprint arXiv:2108.00574 (2021).
- [83] Rotem Arnon-Friedman, Frédéric Dupuis, Omar Fawzi, Renato Renner, and Thomas Vidick, “Practical device-independent quantum cryptography via entropy accumulation,” *Nature com-*

- munications **9**, 1–11 (2018).
- [84] Johan Ahrens, Piotr Badziag, Adán Cabello, and Mohamed Bourennane, “Experimental device-independent tests of classical and quantum dimensions,” *Nature Physics* **8**, 592–595 (2012).
  - [85] It is a particular case of the more general scheme, the star-shape network [52, 65, 94] (Fig. 1 c). In this kind of network  $n$ -nodes are connected to a central one, that is  $n = 2$  for the bilocal case.
  - [86] Armin Tavakoli, Paul Skrzypczyk, Daniel Cavalcanti, and Antonio Acín, “Nonlocal correlations in the star-network configuration,” *Physical Review A* **90**, 062109 (2014).
  - [87] Denis Rosset, Cyril Branciard, Tomer Jack Barnea, Gilles Putz, Nicolas Brunner, and Nicolas Gisin, “Nonlinear Bell inequalities tailored for quantum networks,” *Phys. Rev. Lett.* **116**, 010403 (2016).
  - [88] Nicolas Gisin, Quanxin Mei, Armin Tavakoli, Marc Olivier Renou, and Nicolas Brunner, “All entangled pure quantum states violate the bilocality inequality,” *Physical Review A* **96**, 020304 (2017).
  - [89] Francesco Andreoli, Gonzalo Carvacho, Luca Santodonato, Rafael Chaves, and Fabio Sciarrino, “Maximal qubit violation of  $n$ -locality inequalities in a star-shaped quantum network,” *New Journal of Physics* **19**, 113020 (2017).
  - [90] John F Clauser, Michael A Horne, Abner Shimony, and Richard A Holt, “Proposed experiment to test local hidden-variable theories,” *Physical Review Letters* **23**, 880 (1969).
  - [91] F. Basso Basset, M. B. Rota, C. Schimpf, D. Tedeschi, K. D. Zeuner, S. F. Covre da Silva, M. Reindl, V. Zwiller, K. D. Jöns, A. Rastelli, and R. Trotta, “Entanglement swapping with photons generated on demand by a quantum dot,” *Physical Review Letters* **123**, 160501 (2019).
  - [92] Harishankar Jayakumar, Ana Predojević, Tobias Huber, Thomas Kauten, Glenn S. Solomon, and Gregor Weihs, “Deterministic photon pairs and coherent optical control of a single quantum dot,” *Physical Review Letters* **110**, 135505 (2013).
  - [93] Tobias Huber, Maximilian Prilmüller, Michael Sehner, Glenn S Solomon, Ana Predojević, and Gregor Weihs, “Interfacing a quantum dot with a spontaneous parametric down-conversion source,” *Quantum Science and Technology* **2**, 034016 (2017).
  - [94] Elisa Bäumer, Nicolas Gisin, and Armin Tavakoli, “Demonstrating the power of quantum computers, certification of highly entangled measurements and scalable quantum nonlocality,” *npj Quantum Information* **7**, 1–6 (2021).

## SUPPLEMENTARY MATERIAL

### 1. SPECIFICATIONS OF THE EXPERIMENTAL APPARATUS

#### A. Fiber and free-space quantum channels

As described in the main text, two channels for quantum communication have been employed: a free-space channel ( $\mathcal{C}_{AB}$ ) and a fiber link ( $\mathcal{C}_{BC}$ ) connecting A to B and C to B, respectively.  $\mathcal{C}_{BC}$  connects two measurement stations in the same building using a 25m-long single mode fiber, which has shown losses of 8%. Conversely, the implementation and the characterization of the free-space link  $\mathcal{C}_{AB}$  required more sophisticated considerations. When light propagates in free-space, it is affected by several phenomena. Natural diver-

gence of Gaussian beams spreads light out of its collimation. Then, the beam wandering, due to interaction of light with air masses having random density, continuously changes the beam direction. Reducing these effects requires a trade-off in the choice of beam waist to use. The larger the beam waist, the higher the collimation. Conversely, a reduced spot size of the beam is less affected by beam wander oscillations. In our case we adopted a beam waist diameter of 22 mm, thus providing a Rayleigh range of about 2 km. This is done by a suitable telescope in the sender platform (Fig.4a). The resulting beam wander must be corrected in order to handle the received light and couple it into single mode fiber. In order to achieve this task, we employed an advanced stabilization system: the MRC-Laser Beam Stabilization (by MRC Systems GmbH). It consists of two fast steering mirrors (FSMs) connected to as many position detectors (PDs) and a control unit. This system allows a stabilization of the beam center at frequencies  $< 200$  Hz with accuracy  $< 0.1\mu\text{m}$ , i.e. suitable for single-mode coupling. The entire receiver platform is reported in the Supplementary Fig.4b. The losses of the free-space channel can be minimized by a suitable choice of the signal wavelength. A good compromise for free-space propagation is the infrared region around 800 nm. In our case, we adopted a single-photon signal at 783.2 nm and a further laser at 850 nm, which acts as stabilization control. At these wavelengths, the losses measured along the link in free-space are about 15%. At the sender platform, both the light at 783.2 nm and the laser at 850 nm exit from the same single mode fiber, in order to experience the same perturbations during the air link propagation. Once arrived at the receiver platform, the light is reduced by a telescope similar to the one exploited for the sender platform. The 783.2 nm-signal is divided by the 800 nm-laser through a dichroic mirror (DM), and coupled into a single-mode fiber. This fiber is connected to a further optical table, where the signal is measured according to the protocol described in the main text. Instead the control laser is transmitted by the DM and sent to PDs, thus enabling the active stabilization of the photons affected by the free-space channel.

Additionally, to compensate for slow thermal drifts in the pointing direction of the sender platform and improve long-term stability, a mirror with a piezoelectric mount is inserted after the second lens of its telescope. The motion of the piezoelectric actuators is driven using a custom PID controller. The feedback is given by a compact CMOS camera placed at the receiver’s end which tracks the position of the 850 nm beam. The camera receives the light partially reflected by another DM placed after the second lens of the receiver’s telescope, which transmits the signal at 783.2 nm.

While the experiment is conducted sending single photons at 783.2 nm, the channel characterization and alignment is made by a simulation laser at the same wavelength. Using this laser, the losses were measured and the final losses budget is reported in the Supplementary Table I for all channels used.



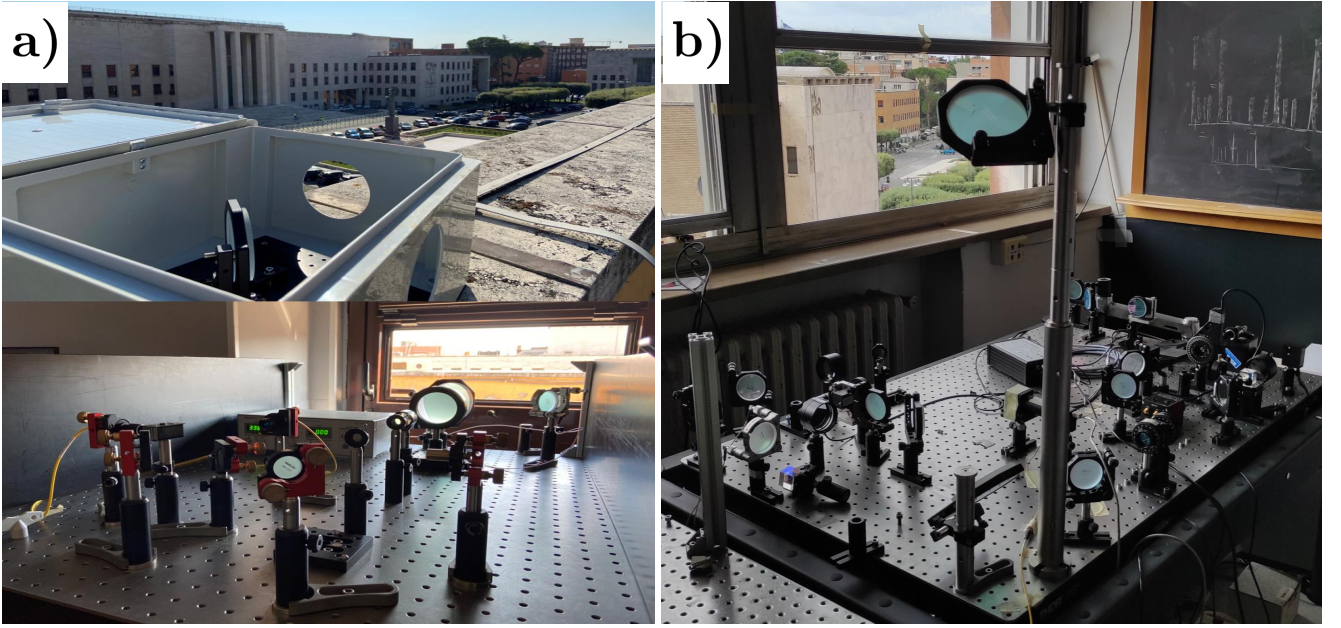


FIG. 4. (a) Transmitter and (b) receiver platforms adopted for the free-space optical link. The platforms are in air-conditioned laboratories to mitigate the impact of environmental effects such as temperature variations. In the transmitter side, a mirror in an external enclosure is placed on the terrace of the building (above) to compensate for the lack of direct line of sight between the two laboratories.

| free-space link                   | Losses |
|-----------------------------------|--------|
| Propagation on sending table      | 15%    |
| Air propagation                   | 15%    |
| Propagation on receiving table    | 20%    |
| SMF coupling of stabilized signal | 50%    |

TABLE I. Main optical losses affecting the signal in the free-space quantum channel. SMF: single mode fiber.

### B. Monolithic SPDC source

The realized source is based on a Sagnac interferometer that generates photon pairs entangled in polarization (see Fig. 5). It is mounted on a breadboard of reduced dimensions and makes use of a cage system in a compact and portable structure. This monolithic architecture demonstrated high stability of the produced signal over time, maintaining stable CHSH violation for over 24 hours. Furthermore, the possibility to be moved to different locations makes it interesting for further network investigation, as it is versatile to change structure geometry. For example, to realize node configurations where spatial loophole can be closed.

### C. Synchronization between the three nodes

During the measurement, the events registered by the single-photon detectors in the three nodes are sorted and timed

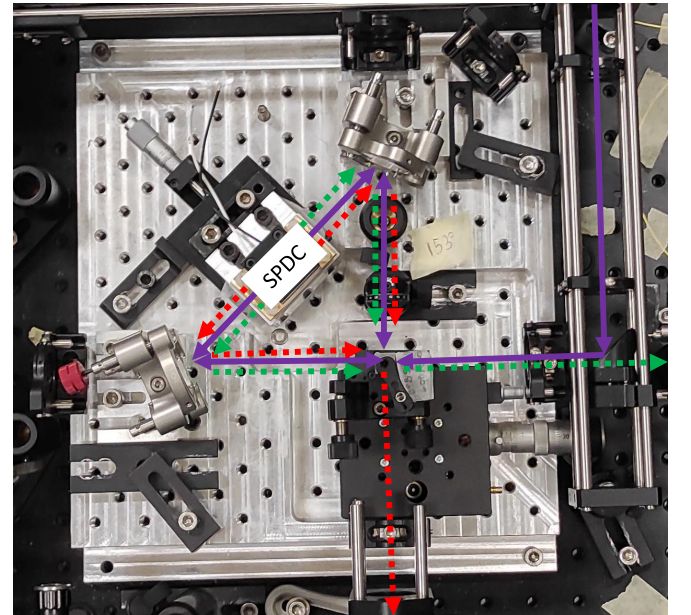


FIG. 5. Picture of the employed Sagnac source of polarization-entangled photon pairs. The pump laser at 405 nm (purple line) generates pairs of photons (green and red dots) through SPDC process in a 2 cm ppKTP<sup>a</sup> non linear crystal. The recombination in the polarizing beam splitter allows the preparation of entangled states of light on the output modes of the interferometer. The monolithic architecture of the source provides high stability of the source performances.

<sup>a</sup> Periodically poled potassium titanyl phosphate

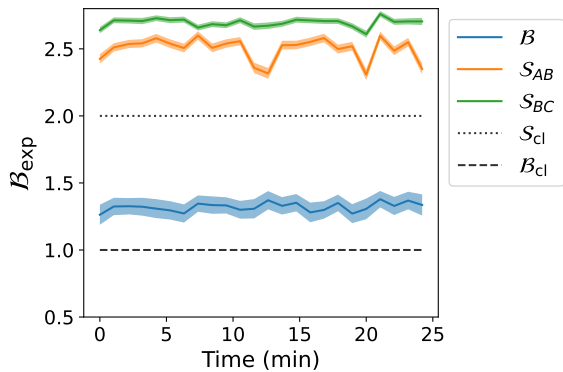


FIG. 6. Experimental violation of bilocality (blue curve) and individual CHSH violations (green and orange curves) are reported as a function of the time ( $\sim 25$  min of acquisition). Coloured shaded regions represent the corresponding standard deviations. Classical bounds are shown for comparison (dashed lines).

by a TDC (Time-to-Digital Converter), with a resolution of 81 ps, and filtered to select only two-fold coincidences between simultaneous detections coming from the same source. Since each of the three nodes features its own independent TDC, a common time reference is needed for the proper synchronization of the devices.

The solutions used in our work are different for the two channels, i.e. the fiber link and the free-space one. In particular, while for the former a common clock signal is directly shared between the two TDCs via coaxial cables, for the latter the larger distance that separates the stations makes this more problematic. We have solved it by resorting to two independent GPS-locked oscillators generating a reference signal, and then using the photon coincidences themselves to obtain the required sub-ns accuracy. In this way, we also demonstrate the feasibility of this last synchronization method, which can

be effectively deployed in a wide variety of situations, where direct cabling is unavailable. In the following we give a brief description of the synchronization procedure.

The GPS-locked oscillators are located in stations A and B, and are configured to send two different TTL signals: a 10 kHz square wave and a short pulse at 1 Hz to their respective TDCs. The former signal is necessary to correct the drift of the internal TDC clock, while the latter represents the actual common clock. Node B shares these signals directly with C, which already gives an accurate synchronization between these two nodes. Node A instead relies on the GPS-locking between the signals in A and B which allows for a coarse synchronization up to  $\approx 10$ -20 ns.

The fine correction to the delays between node A, B and C are then performed by choosing two reference detectors, where two-fold coincidences are expected, and by looking at the highest peak in the histogram of the time differences between their detection events. The GPS synchronization described earlier allows us to efficiently perform this computation by restricting the histogram to a small region ( $\pm 40$  ns) around the coarse value for the delay, which makes the procedure fast enough to be done in realtime while the measurement is running.

## 2. EXPERIMENTAL VIOLATION OF THE BILOCAL SCENARIO

As reported in the main text, during the experiment on the tripartite system four-fold coincidences are employed to compute the bilocal parameter, while two-fold events to monitor the corresponding CHSH violations. Supplementary Figure 6 shows such parameters as a function of time and the stability of the network performances.